Supplementary Information

Table of contents

A. Supplementary figures

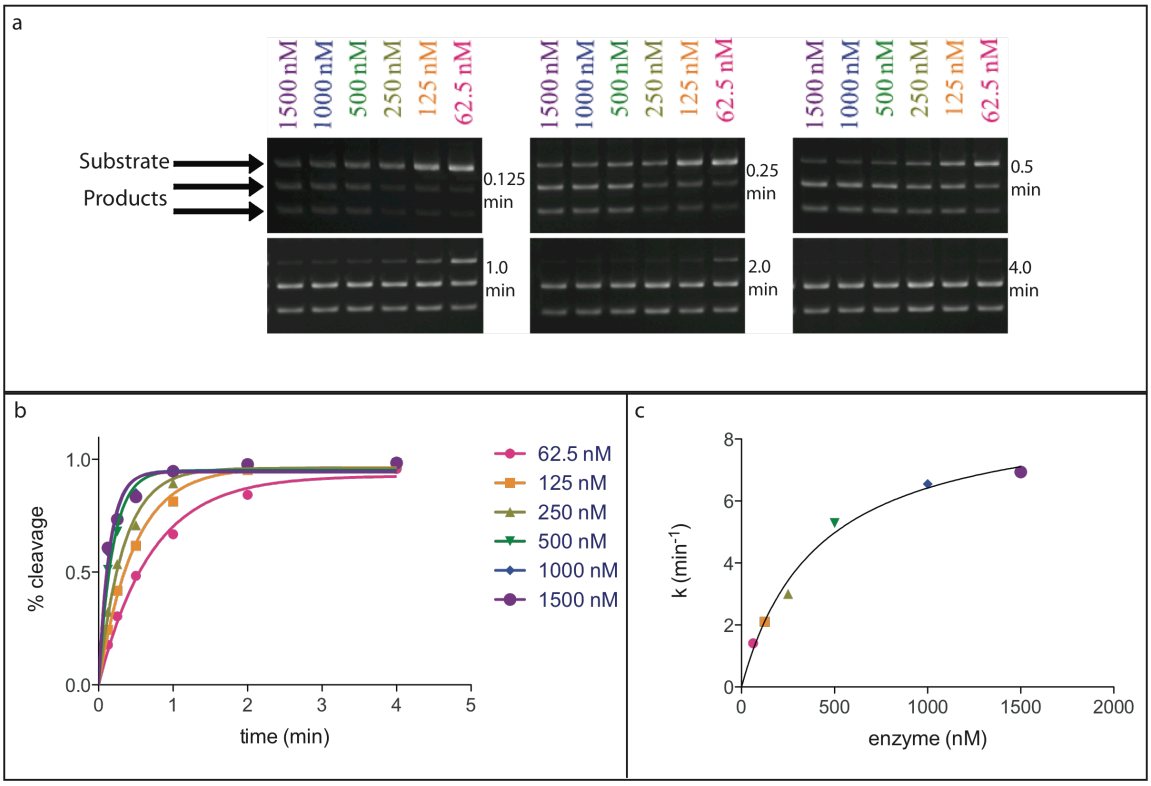

Figure S1. a) Example of a kinetic assay on a 1.2% agarose TBE gel. Six time-points were collected over a 24-fold range of enzyme concentrations. **b)** The percent cleavage was calculated by integrating the densities of the bands in a) using ImageJ, and dividing the sum of the densities of the two product bands by the sum of the densities of all three bands. The percent cleavage for each enzyme concentration was plotted versus time using GraphPad Prism, and the rate was determined by fitting to a single-exponential function. **c)** The rate from each of the time-courses in b plotted versus enzyme concentration with Michaelis-Menten fits to determine the parameters k_{cat}* and K_M*.

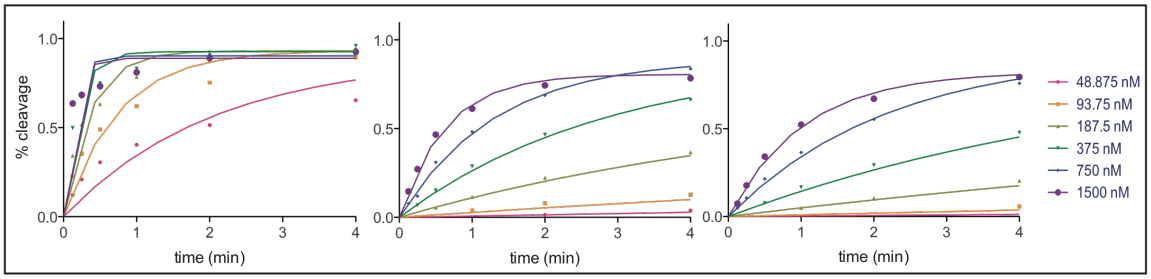

Figure S2. Three single base-pair variants in the central four base pairs from the wild-type target site display behavior that cannot be fit with a single-exponential (-2A, -1C, and +1A) when kinetics are collected with wild-type and Y2 I-AniI (data not shown). (Left plot) wild-type enzyme (not Y2) cleaving the LIB4 target site – a variant site with increased binding affinity that includes the +1A mutation (as well as the +8T mutation)[1] – cannot be fit with a single-exponential. (Middle plot) the original wild-type enzyme

cleaving the LIB4 target site with an additional -9A substitution can be fit with a single-exponential. The -9A target site has significantly increased K_M* compared to the wild-type target site. (Right plot) the -9C:G designed enzyme cleaving the LIB4 target site (not containing the intended -9C substitution) can be fit with a single-exponential. The deviation from simple exponential kinetics evidently is a function of the interaction between the enzyme and target site. A comparison of the left and middle plots indicate that the deviation is not inherent in the enzyme, and comparison of the left and right plots indicate that it is not inherent in the LIB4 target site. The deviations from single exponential kinetics could result from a non-productive mode of binding or a slow DNA conformational change, for several of the substituted central four substrates (-2A, -1C, +1A), that is only evident when the target site is tightly bound by the enzyme (both the middle and right plots are under conditions of suboptimal binding).

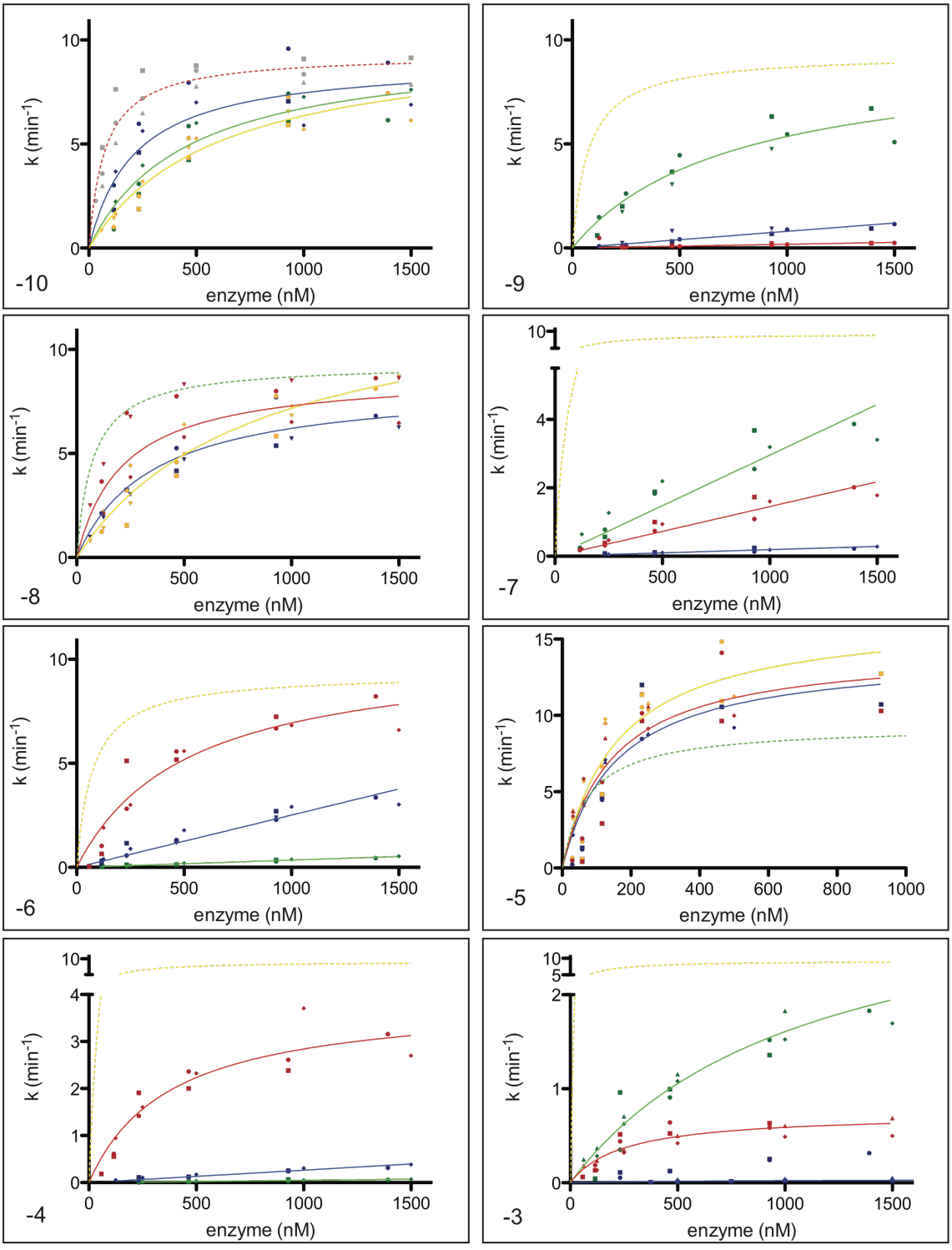
-10
-9
-8
-7
-6
-5
-4
-3
k (min-1)
enzyme (nM)

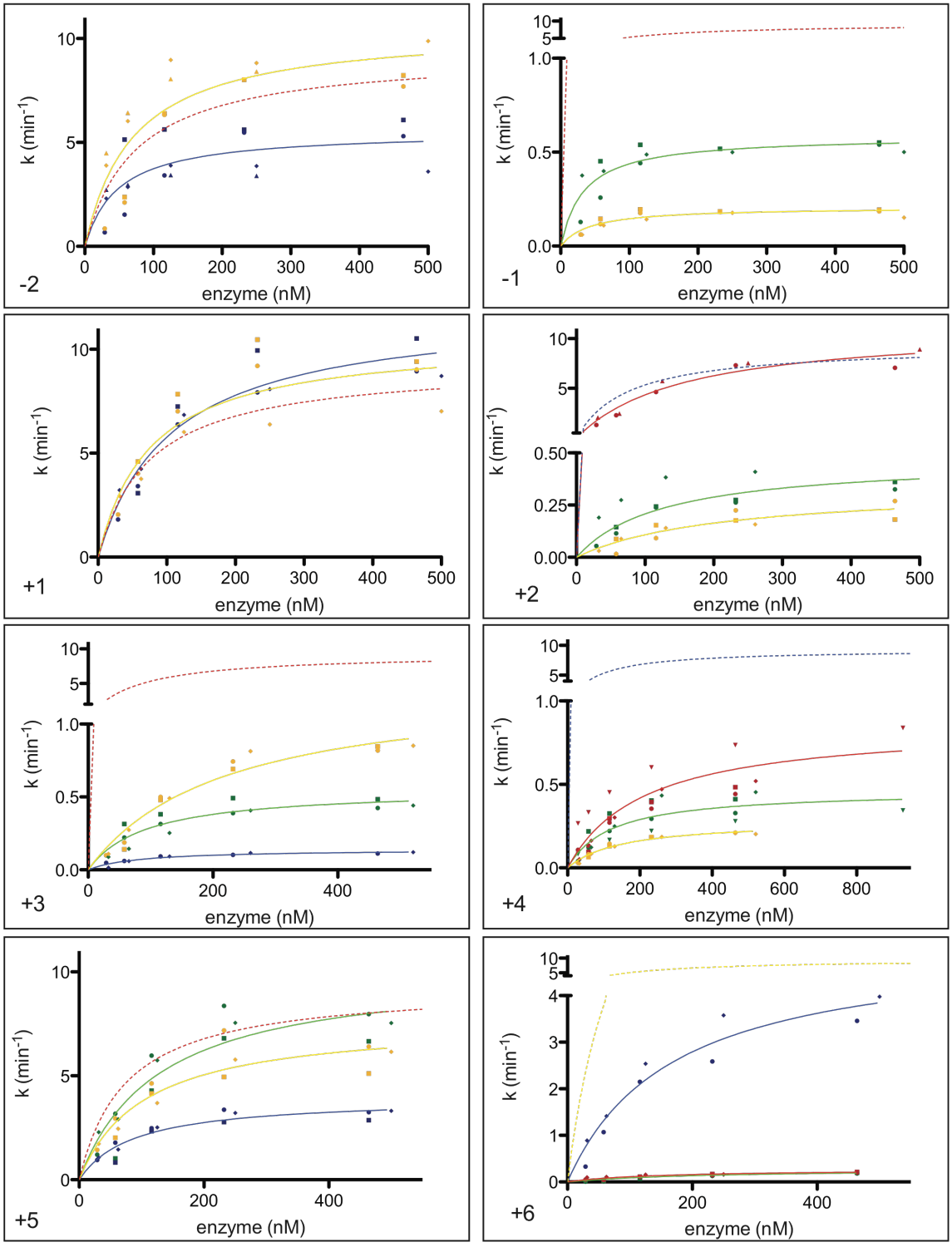
-2
k (min-1)
enzyme (nM)
-1
k (min-1)
enzyme (nM)
+1
k (min-1)
enzyme (nM)
+2
k (min-1)
enzyme (nM)
+3
k (min-1)
enzyme (nM)
+4
k (min-1)
enzyme (nM)
+5
k (min-1)
enzyme (nM)
+6
k (min-1)
enzyme (nM)

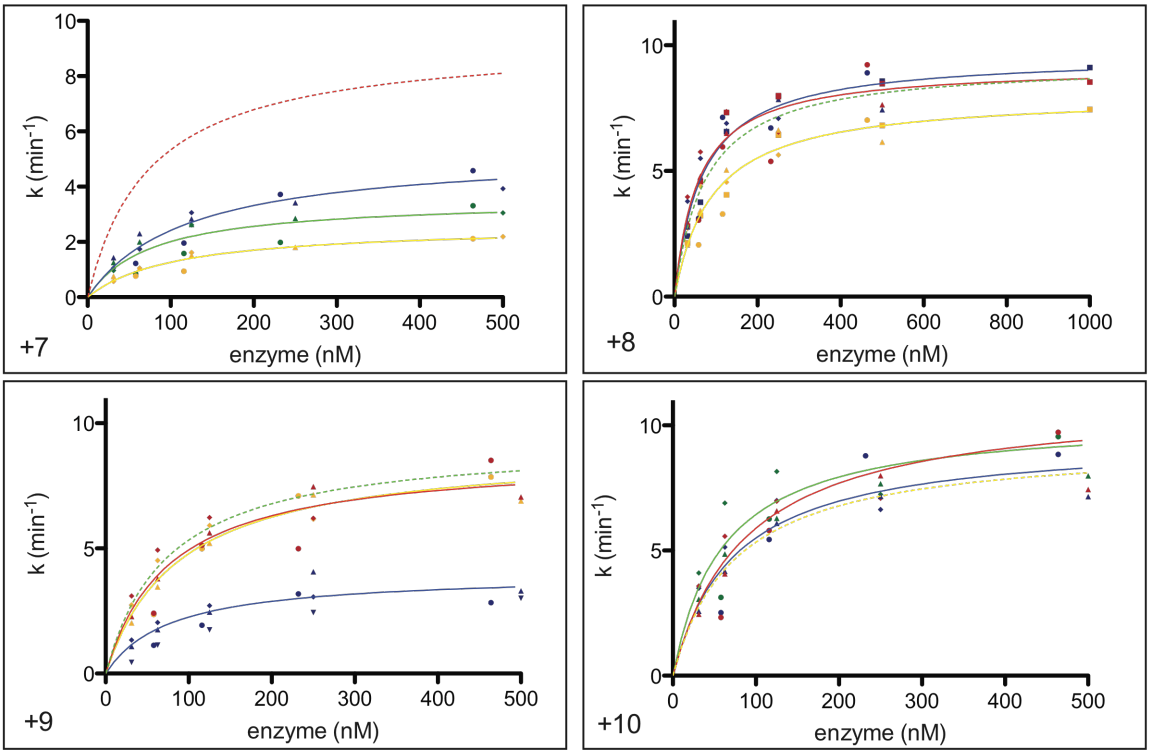

Figure S3. Michaelis-Menten plots for each of the 60 singly-substituted target sites in order from left to right across the target site. The data is grouped by position and colored by nucleotide (A=green, C=blue, G=yellow, T=red). The Michaelis-Menten curve fit for the wild-type target site is included on every graph as a dashed line with the color of the wild-type base-pair at that position; the actual data points for the wild-type substrate are shown only in the -10 position panel (grey).

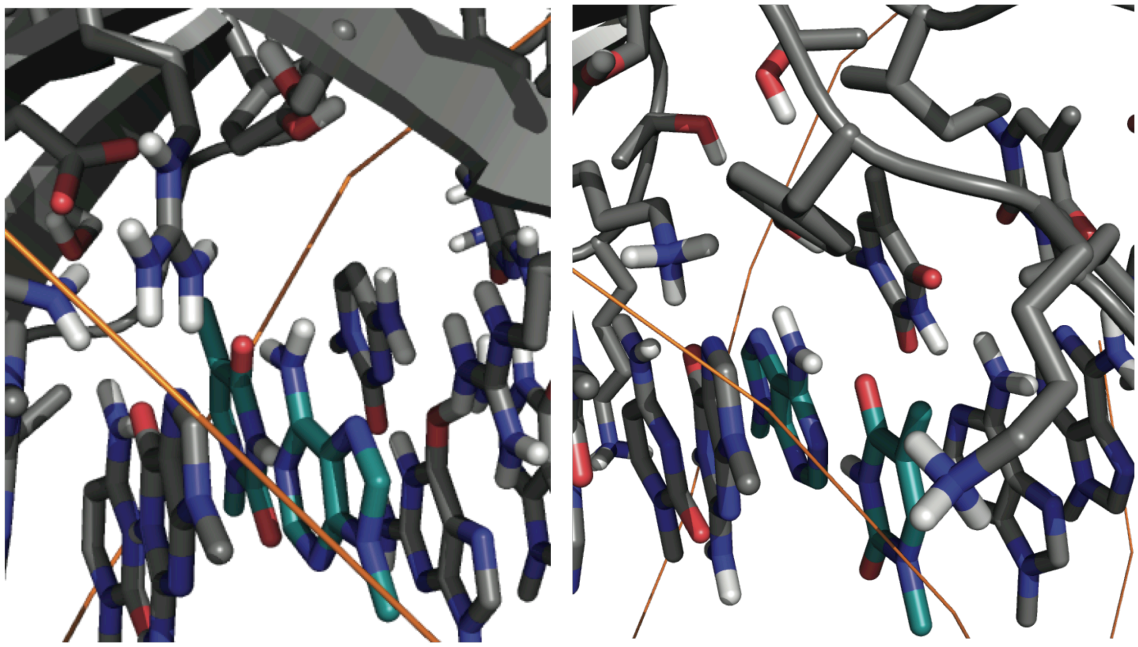

Figure S4. The -5 position (left panel) and +7 position (right panel) do not make obvious

contacts in the crystal structure. The -5 position has both an increased k_{cat}* and K_M* / K_A, and the +7 (as well as several other positions) has both a decreased k_{cat}* and K_A (K_M* values smaller than wild-type are difficult to determine accurately). This is consistent with removal or creation of interactions that are present in the Michaelis complex but not the transition state complex, and we predict these base-pairs make more extensive interactions in the Michaelis complex than in the transition state.

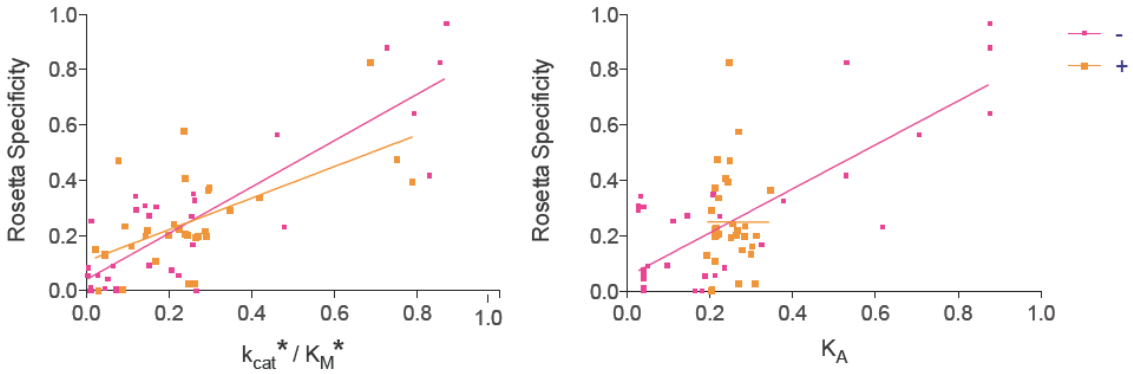

Figure S5. Correlation between predicted and observed specificity for k_{cat}* / K_M* (left panel) and K_A (right panel). Specificity is defined as $e^{(-\Delta Xwt/t)} / \sum e^{(-\Delta Xall/t)}$ (where the numerator is the single base-pair of interest and the denominator is the sum of all four base-pairs at the position); t is set to 1.5. For the Rosetta computed specificities, ΔX in the numerator is the protein-DNA interaction energy, and in the denominator the sum is over all four basepairs at the position. For the experimental specificity determinations, ΔX is defined as $\Delta\ln(k_{cat}* / K_M*)$ (left panel) or $\Delta\ln(K_A)$ (right panel) for each substitution compared to wild-type. The correlation is significantly stronger for k_{cat}* / K_M* with Rosetta specificity (R^2=0.74 for left (-) side and 0.38 for right (+) side) than for K_A with Rosetta specificity (R^2=0.66 for left (-) side and 0.00 for right (+) side), supporting the idea that the crystal structure more closely resembles the transition state of the reaction than it does the ground state complex.

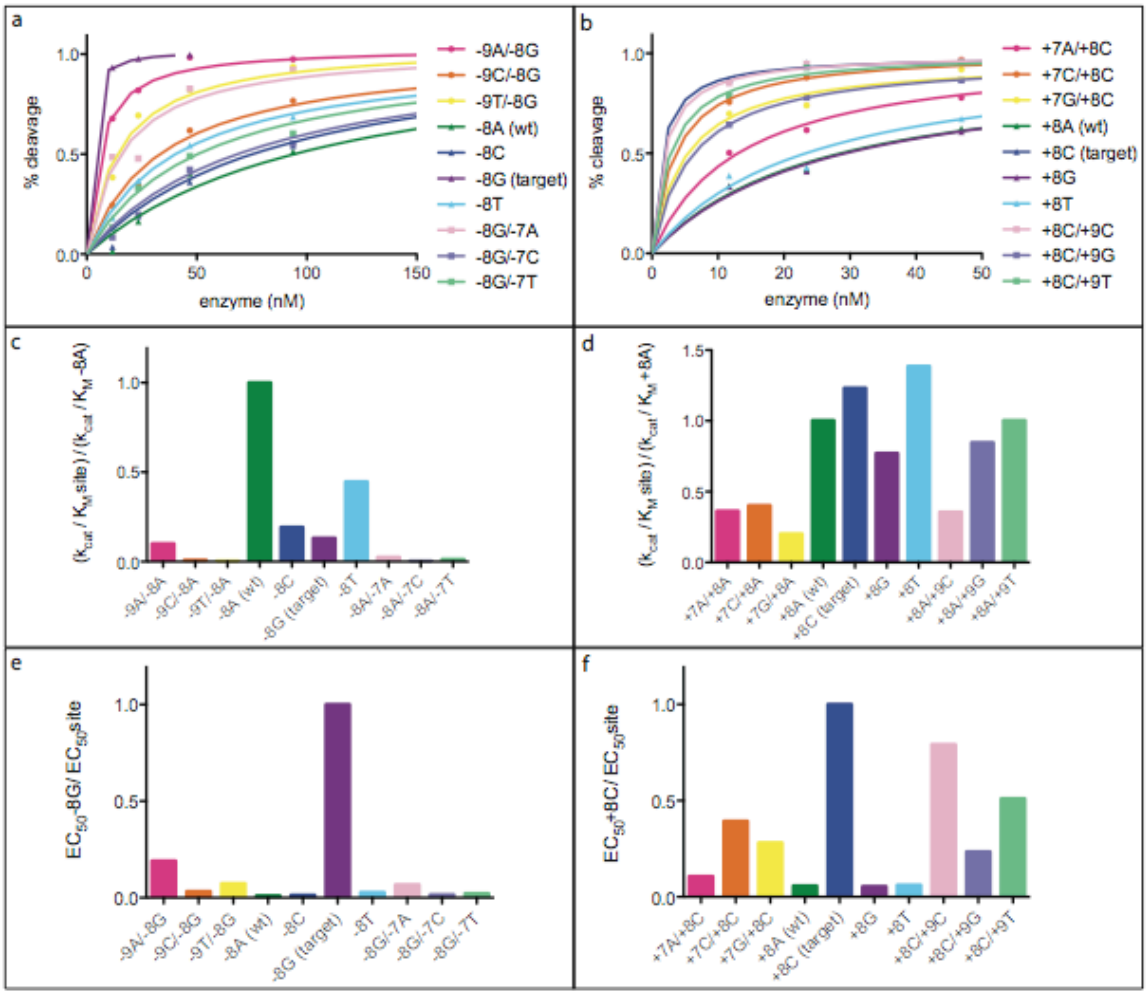

Figure S6. Specificity at positions adjacent to the designed base-pair for the -8G:C_A and +8C:G designs. **a)** and **b**): percent cleavage by the -8G:C_A (a) and +8C:G (b) designed enzymes as a function of enzyme concentration. **c)** and **d)**: specificity of Y2 (c) and designed enzyme (e) at positions surrounding -8G:C_A; **d)** and **f)**: specificity of Y2 (d) and designed enzyme (f) at positions neighboring +8C:G. Specificity for Y2 (c) and (d) is determined by ratios of k_{cat}* / K_M* (Table S1). Specificity for designed enzymes -8G:C_A (e) and +8C:G is determined by ratios of EC_{50} values from (a) and (b). Comparison of c) and d) with e) and f) shows that the overall specificity of both designed endonucleases is increased over the Y2 starting point.

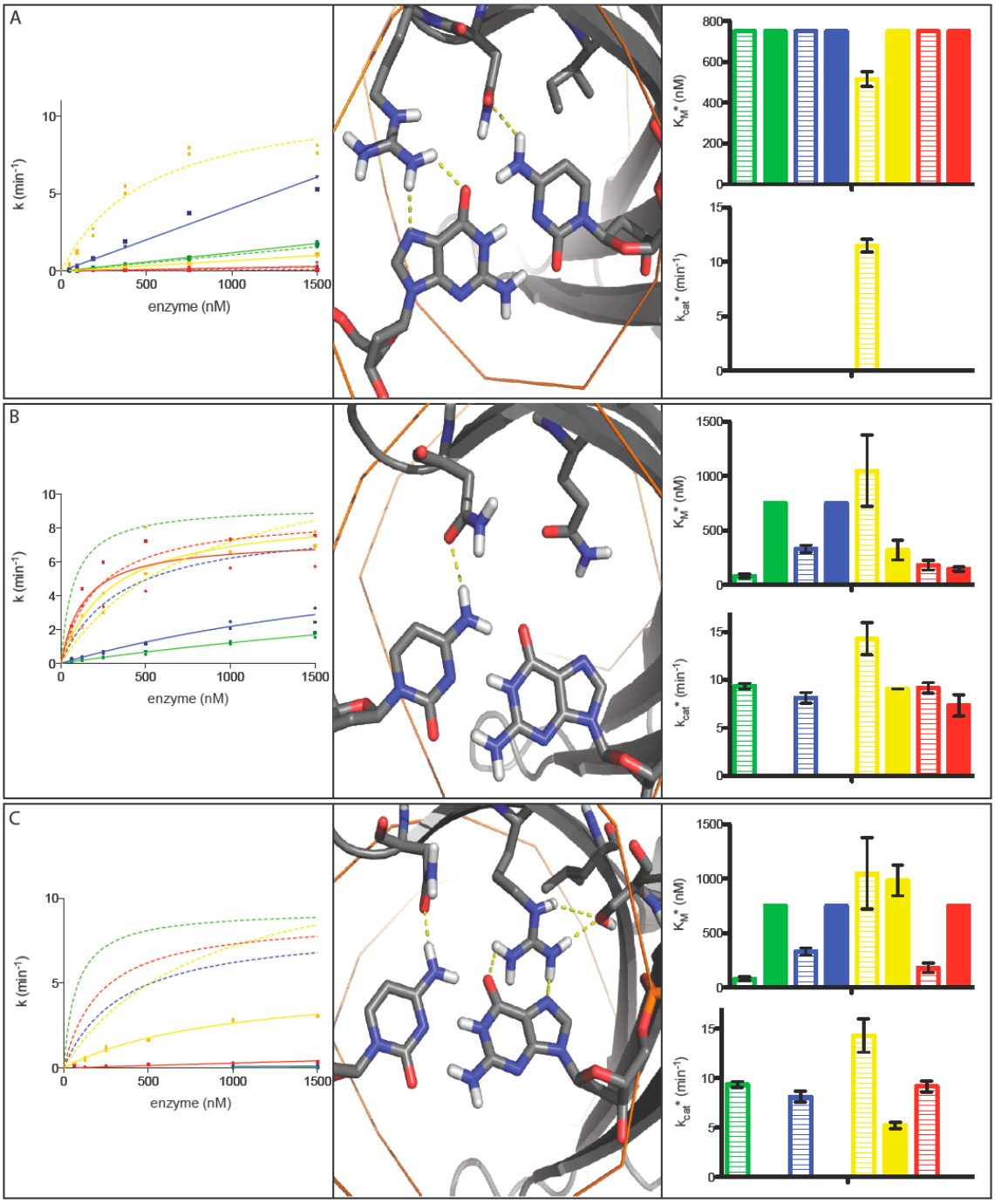
A
k (min-1)
enzyme (nM)
KM* (nM)
kcat* (min-1)
B
k (min-1)
enzyme (nM)
KM* (nM)
kcat* (min-1)
C
k (min-1)
enzyme (nM)
KM* (nM)
kcat* (min-1)

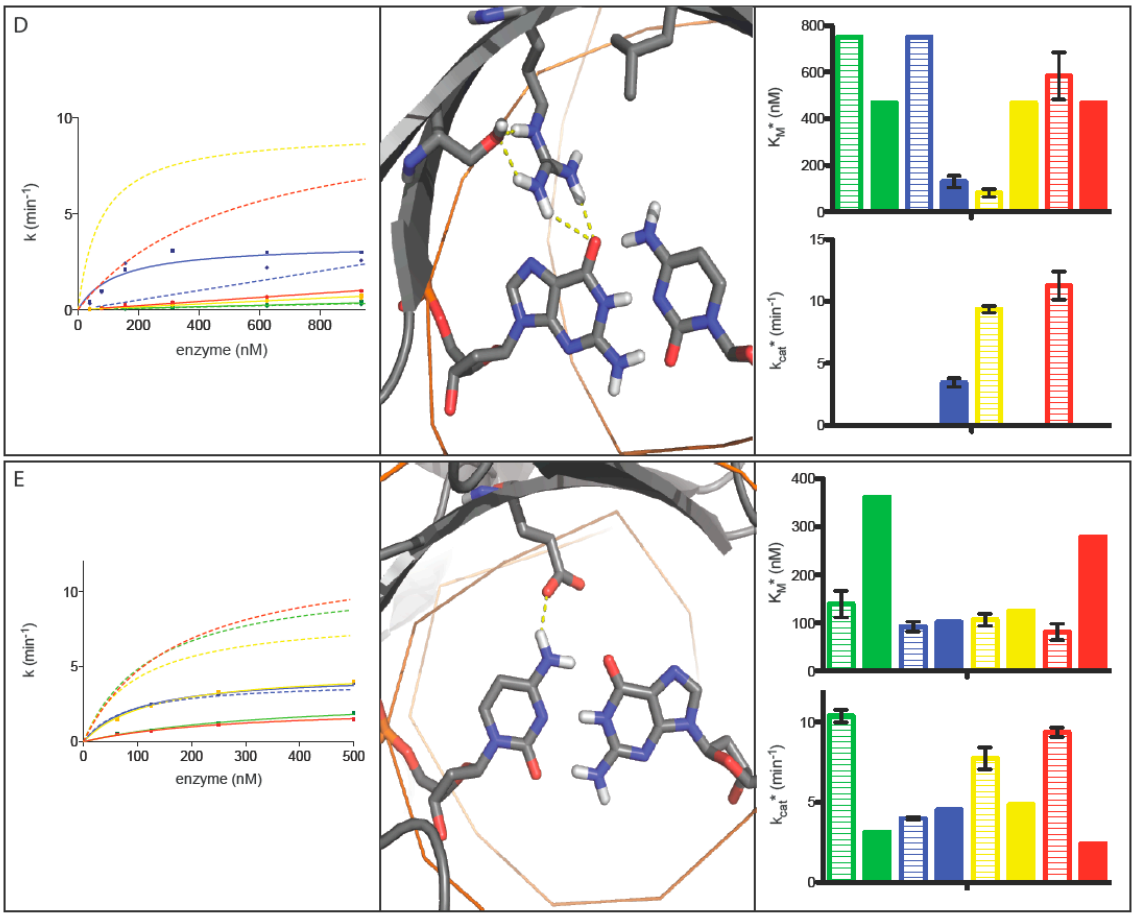

Figure S7. The color scheme throughout the figure is A=green, C=blue, G=yellow,T=red, and error bars in right panels are standard errors from the mean (SEM). **a)** Design for -9G:C to -9C:G substitution (K24N, G25R, T29I). (Middle panel) The designed residue R25 makes hydrogen bonds to -9G, and N24 makes a hydrogen bond to -9C. I29 removes contacts with the wild-type -9G:C and provide space for the new contacts provided by R25 and N24. (Left panel, right panel) this enzyme overall binds significantly more poorly than wild-type enzyme, in part because it is missing the Y2 mutations that enhance binding (due to expression issues with the Y2 version of this design). However, the enzyme is specific for the designed site, which was not tolerated at all by the wild-type enzyme, and the specificity appears to be derived from modulation of K_M*. **b)** Design B for -8A:T to -8G:C substitution (K24N, T29Q). (Middle panel) The designed residue N24 makes hydrogen bonds to -8C (as in the other two designs for this same base-pair). (Left panel, right panel) this design is equally specific for the -8T:A and the target -8G:C, however it has significantly increased K_M* for the other two substitutions (the altered specificity is achieved through K_M*, not k_{cat}*). **c)** Design C for -8A:T to -8G:C substitution (K24N, T29R, E31L, R72S). (Middle panel) The designed residue R29 makes hydrogen bonds to -8G, and N24 makes hydrogen bonds to -8C (as in the other two designs for this same base-pair). S72 is positioning R29 and L31 is necessary to allow space for R29 to contact -8G (additional, it is likely electrostatic influences of E31 would have disrupted the R29 contact). (Left panel, right panel) this enzyme overall binds significantly more poorly than wild-type enzyme. However, the

enzyme is very specific for the designed site over the other three possible target sites (significantly more specific than the wild-type enzyme at this position) and the specificity appears to be derived from modulation of K_M*****. **d)** Design for -6G:C to -6C:G substitution (T29S, E31R, R70L). (Middle panel) The designed residue R31 makes direct hydrogen bonds to -6G, and its position is stabilized by hydrogen bonds with S29. The L70 mutation is necessary to remove direct interactions with the wild-type base-pair at this position. (Left panel, right panel) this enzyme overall binds significantly more poorly than wild-type enzyme. However, the enzyme is very specific for the designed site over the other three possible target sites. **e)** Design for +5T:A to +5C:G substitution (D168E). (Middle panel) the designed residue E168 makes a direct hydrogen bond with +5C. (Left panel, right panel) the shifts in activity for this enzyme results mainly from modulation of k_{cat}***** and a switching of the order of k_{cat}***** preferences at this position, resulting in enhanced specificity over the wild-type enzyme.

B. Supplementary tables

Table S1. Kinetic parameters for singly-substituted sites. *

position	base-pair	k_{cat}* / K_M*	k_{cat}* (min^{-1})	K_M* (nM)	Relative K_A
wild-type	wild-type	0.13 ± 0.04	9.4 ± 0.3	81 ± 17	1.0
-10T	A	0.021 ± 0.004	10.0 ± 0.5	505 ± 120	-0.073 ± 0.030
	C	0.052 ± 0.014	9.4 ± 1.2	219 ± 70	0.38 ± 0.03
	G	0.017 ± 0.002	11.4 ± 1.2	748 ± 157	-0.054 ± 0.040
-9G	A	0.013 ± 0.003	10.5 ± 1.9	946 ± 294	-0.23 ± 0.03
	C	0.0010 ± 0.0001	-	>750	-0.16 ± 0.06
	T	0.00020 ± 0.00002	-	>750	-0.28 ± 0.03
-8A	C	0.025 ± 0.002	8.1 ± 0.6	330 ± 34	0.051 ± 0.048
	G	0.017 ± 0.004	14.3 ± 1.7	1048 ± 328	-0.078 ± 0.018
	T	0.058 ± 0.014	9.2 ± 0.6	180 ± 49	-0.11 ± 0.02
-7G	A	0.003 ± 0.0004	-	>750	-0.13 ± 0.04
	C	0.00020 ± 0.00003	-	>750	-0.17 ± 0.06
	T	0.0016 ± 0.0002	-	>750	-0.17 ± 0.02
-6G	A	0.00035 ± 0.00002	-	>750	-0.22 ± 0.02
	C	0.0030 ±0.0001	-	>750	-0.071 ± 0.045
	T	0.020 ± 0.002	11.3 ± 1.1	583 ± 102	-0.087 ± 0.010
-5A	C	0.104 ± 0.009	13.0 ± 0.8	129 ± 19	0.36 ± 0.06
	G	0.130 ± 0.032	15.6 ± 1.1	144 ± 49	0.41 ± 0.05
	T	0.13 ± 0.04	14.3 ± 1.5	153 ± 60	0.46 ± 0.09
-4G	A	0.000053 ± 0.000009	-	>750	0.26 ± 0.02
	C	0.00027 ± 0.00001	-	>750	0.098 ± 0.05
	T	0.0104 ± 0.0007	3.8 ± 0.2	374 ± 40	0.15 ± 0.04
-3G	A	0.003 ± 0.001	3.4 ± 0.6	1134 ± 317	0.20 ± 0.06
	C	0.00007 ± 0.00003	0.046 ± 0.008	874 ± 204	0.30 ± 0.04
	T	0.0028 ± 0.0003	0.78 ± 0.06	281 ± 29	0.030 ± 0.033
-2T	A	-	-	-	1.84 ± 0.25
	C	0.28 ± 0.11	5.4 ± 1.0	53 ± 39	1.12 ± 0.05
	G	0.17 ± 0.05	10.6 ± 0.3	86 ± 26	2.14 ± 0.12
-1T	A	0.03 ± 0.01	0.58 ± 0.04	36 ± 23	1.66 ± 0.05
	C	-	-	-	0.60 ± 0.05
	G	0.006 ± 0.002	0.20 ± 0.009	39 ± 10	2.05 ± 0.09
+1T	A	-	-	-	1.76 ± 0.12
	C	0.12 ± 0.01	12.1 ± 1.3	109 ± 19	1.28 ± 0.13
	G	0.15 ± 0.01	10.6 ± 1.3	74 ± 12	1.67 ± 0.36
+2C	A	0.03 ± 0.02	0.38 ± 0.05	81 ± 39	1.49 ± 0.15
	G	0.003 ± 0.001	0.23 ± 0.02	97 ± 31	1.89 ± 0.35
	T	0.071 ± 0.002	11.2 ± 1.0	157 ± 11	0.34 ± 0.06
+3T	A	0.0030 ± 0.0004	0.56 ± 0.03	104 ± 42	1.63 ± 0.12
	C	0.002 ± 0.001	0.14 ± 0.02	84 ± 34	0.83 ± 0.08
	G	0.0060 ± 0.0003	1.3 ± 0.03	222 ± 17	1.49 ± 0.03
+4C	A	0.004 ± 0.001	0.51 ± 0.07	150 ± 36	1.02 ± 0.06
	G	0.0020 ± 0.0002	0.32 ± 0.04	185 ± 39	1.35 ± 0.13
	T	0.005 ± 0.001	0.75 ± 0.06	171 ± 27	0.77 ± 0.08
+5T	A	0.080 ± 0.013	10.4 ± 0.4	139 ± 28	1.87 ± 0.31
	C	0.045 ± 0.006	4.0 ± 0.09	92 ± 10	1.07 ± 0.12
	G	0.074 ± 0.007	7.7 ± 0.7	106 ± 12	1.52 ± 0.16
+6G	A	0.00100 ± 0.00007	0.45 ± 0.002	614 ± 51	1.19 ± 0.06
	C	0.031 ± 0.006	5.1 ± 0.2	170 ± 24	1.14 ± 0.12
	T	0.00120 ± 0.00006	0.34 ± 0.034	282 ± 41	0.74 ± 0.14
+7T	A	0.047 ± 0.016	4.5 ± 0.6	157 ± 91	1.25 ± 0.13
	C	0.052 ± 0.014	5.8 ± 1.0	147 ± 68	0.94 ± 0.02
	G	0.026 ± 0.006	2.9 ± 0.3	134 ± 47	1.68 ± 0.18
+8A	C	0.16 ± 0.03	9.5 ± 0.5	68± 15	1.18 ± 0.06
	G	0.10 ± 0.03	8.3 ± 1.0	118 ± 51	1.54 ± 0.25
	T	0.18 ± 0.05	9.5 ± 0.8	74 ± 28	1.38 ± 0.11
+9A	C	0.046 ± 0.01	3.9 ± 0.2	96 ± 18	1.42 ± 0.26
	G	0.11 ± 0.03	9.1 ± 1.0	96 ± 30	1.29 ± 0.14

	T	0.13 ± 0.04	9.4 ± 1.3	108 ± 53	1.41 ± 0.22
+10A	A	0.20 ± 0.07	10.6 ± 1.6	71 ± 31	1.04 ± 0.11
	C	0.15 ± 0.04	9.8 ± 1.5	85 ± 37	1.06 ± 0.13
	T	0.15 ± 0.04	11.0 ± 2.1	90 ± 39	1.00 ± 0.10

[*] All values are the mean ± the standard error from mean (SEM) from 2-4 independent reaction velocity versus enzyme concentration experiments.

Table S2. Kinetic parameters for designed enzymes*

Design	Mutations	Base-pair†	WT k_{cat}* (min^{-1})	WT K_M* (nM)	WT k_{cat}* / K_M*	Variant k_{cat}* (min^{-1})	Variant K_M* (nM)	Variant k_{cat}* / K_M*	Exp. Spec.	Pred. Spec.
-9G:C to -9C:G‡§	K24N, G25R, T29I, F80K**, L233K**	A	-	>750	0.0010 ± 0.00002	-	>750	0.00100 ± 0.00006	0.53	0.28
		C	-	>750	0.00020 ± 0.000005	-	>750	0.0040 ± 0.0002		
		G	11.5 ± 0.6	516 ± 37	0.022 ± 0.0004	-	>750	0.00070 ± 0.00005		
		T	-	>750	0.000071 ± 0.000001	-	>750	0.0002 ± 0.0001		
-8A:T to -8G:C_A	K24N, T29K	A	9.4 ± 0.3	81 ± 17	0.13 ± 0.04	8.3 ± 0.1	2237 ± 17	0.00400 ± 0.00008	0.87	0.96
		C	8.1 ± 0.6	330 ± 34	0.025 ± 0.002	6.0 ± 0.9	1821 ± 466	0.0030 ± 0.0004		
		G	14.3 ± 1.7	1048 ± 328	0.017 ± 0.004	9.9 ± 0.01	26 ± 4	0.40 ± 0.06		
		T	9.2 ± 0.6	180 ± 49	0.058 ± 0.014	9.7 ± 0.9	1535 ± 117	0.0060 ± 0.001		
-8A:T to -8G:C_B	K24N, T29Q	A	9.4 ± 0.3	81 ± 17	0.13 ± 0.04	-	>750	0.00100 ± 0.00009	0.37	0.42
		C	8.1 ± 0.6	330 ± 34	0.025 ± 0.002	-	>750	0.0020 ± 0.0002		
		G	14.3 ± 1.7	1048 ± 328	0.017 ± 0.004	9.06 ± 0.01	320 ± 90	0.031 ± 0.009		
		T	9.2 ± 0.6	180 ± 49	0.058 ± 0.014	7.4 ± 1.1	144 ± 20	0.053 ± 0.015		
-8A:T to -8G:C_C‡	K24N, T29R, R72S, E31L, F80K**, L233K**	A	9.4 ± 0.3	81 ± 17	0.13 ± 0.04	-	>750	0.000025 ± 0.0000005	0.82	0.58
		C	8.1 ± 0.6	330 ± 34	0.025 ± 0.002	-	>750	0.000073 ± 0.000047		
		G	14.3 ± 1.7	1048 ± 328	0.017 ± 0.004	5.2 ± 0.3	983 ± 141	0.0050 ± 0.0004		
		T	9.2 ± 0.6	180 ± 49	0.058 ± 0.014	-	>750	0.00028 ± 0.00001		
-6G:C to -6C:G‡	T29S, E31R, R70L, L233K**	A	-	>750	0.00035 ± 0.00002	-	>469	0.00040 ± 0.00008	0.79	0.94
		C	-	>750	0.0030 ±0.0001	129 ± 25	3.5 ± 0.4	0.027 ± 0.003		
		G	9.4 ± 0.3	81 ± 17	0.13 ± 0.04	-	>469	0.00100 ± 0.00008		
		T	11.3 ± 1.1	583 ± 102	0.020 ± 0.002	-	>469	0.00100 ± 0.000002		
-3G:C to -3C:G	Y18W, E35K, R61Q, L233K**	A	3.4 ± 0.6	1134 ± 317	0.0030 ± 0.0004	6.3 ± 1.2	3070 ± 732	0.00200 ± 0.00008	0.61	0.81
		C	0.046 ± 0.008	874 ± 204	0.00007 ± 0.00003	2.1 ± 0.1	173 ± 5	0.0120 ± 0.0001		
		G	9.4 ± 0.3	81 ± 17	0.13 ± 0.04	6.3 ± 0.5	6261 ± 638	0.00100 ± 0.00003		
		T	0.78 ± 0.06	281 ± 29	0.0028 ± 0.0003	0.46 ± 0.12	730 ± 259	0.00070 ± 0.00007		
+5T:A to +5C:G	D168E, F80K**, L233K**	A	10.4 ± 0.4	139 ± 28	0.080 ± 0.013	3.3 ± 0.2	644 ± 283	0.006 ± 0.002	0.41	0.22
		C	4.0 ± 0.09	92 ± 10	0.045 ± 0.006	4.6 ± 0.1	159 ± 58	0.033 ± 0.012		
		G	7.7 ± 0.7	106 ± 12	0.074 ±	4.8 ± 0.1	283 ± 158	0.025 ±		

* All values are the mean ± the standard error from mean (SEM) from 2-4 independent reaction velocity versus enzyme concentration experiments.
† The wild-type base-pair is highlighted in green and the target base-pair highlighted in cyan.
‡ These enzymes were impure and the concentration of enzyme was calculated using the SDS-PAGE method described in the supplementary material.
§ This variant was tested in the wild-type background with the LIB4 target site due to expression issues with the Y2 version. The enhanced binding of the LIB4 target site[1] compensated for the binding loss associated with missing the Y2 mutations.
** These mutations were included for solubility. Whether or not an enzyme contains these mutations was a function of date of gene construction.

					0.007			0.014		
		T	9.4 ± 0.3	81 ± 17	0.13 ± 0.04	2.7 ± 0.3	779 ± 500	0.005 ± 0.003		
+8A:T to +8C:G	L156Q, I164R, T189S, F80K**, L233K**	A	9.4 ± 0.3	81 ± 17	0.13 ± 0.04	1.1 ± 0.1	169 ± 22	0.007 ± 0.001	0.57	0.83
		C	9.5 ± 0.5	68± 15	0.16 ± 0.03	9.9 ± 0.7	83 ± 3	0.118 ± 0.004		
		G	8.3 ± 1.0	118 ± 51	0.10 ± 0.03	0.89 ± 0.18	78 ± 52	0.018 ± 0.009		
		T	9.5 ± 0.8	74 ± 28	0.18 ± 0.05	1.3 ± 0.2	147 ± 32	0.0090 ± 0.0007		

C. Two-stage DNA binding and domain dominance

The kinetic analyses presented in this paper suggests that in the ground state the interactions on the left side of the interface are largely intact, but those on the right side largely unformed. In the initial binding event, formation of the interactions on the left side may lead to a misalignment of the interactions on the right side, and a conformational change on either the DNA, enzyme, or both may be necessary to form the right side interactions. While a crystal structure of unbound I-AniI has not been determined, there such a structure of the monomeric endonuclease I-DmoI[2]; this structure is virtually identical to that in the complex with target site[3], suggesting that there is unlikely to be large structural changes in the enzyme during catalysis. In contrast, the target site in the I-AniI protein-DNA complex is bent considerably away from B-form conformation, and the enzyme displays a high enthalpic cost of protein-DNA binding which is likely associated with DNA deformation.[4] Yeast display experiments show that the enzyme binds more tightly to the (-) side than to the (+) side (JJ, BLS and AMS, submitted).

These findings are reminiscent of the concept of "domain dominance" described by Silva and coworkers[5] for I-DmoI. In this study it was found that C-terminal domain of the endonuclease loses significant specificity in the presence of Mn^{2+}, cleaving a palindromic target site containing a duplicated (-) half-site, while the N-terminal (A) domain maintains the same specificity in both Mn^{2+} and Mg^{2+}. Additionally, an engineered fusion of two N-terminal (A) domains of I-DmoI retains specificity throughout the entire target site in the presence of Mn^{2+}. Although the two subunits of I-AniI are optimized for different roles in DNA cleavage, the endonuclease maintains a very similar cleavage profile throughout the entire target site in both Mg^{2+} and Mn^{2+} (Michelle Scalley-Kim and Barry Stoddard, unpublished).

Additional monomeric LAGLIDADG endonucleases have also been demonstrated to display strong asymmetry in their binding affinity towards individual DNA half-sites, and/or significant difference in cleavage of those site's corresponding scissile phosphates. The yeast homing endonuclease I-SceI has higher affinity for binding to the 3' DNA half-site, leading to accumulation of nicked intermediates during the cleavage reaction.[6] Similarly, the algal endonuclease I-CpaI preferentially nicks the bottom strand of its target site under limiting concentrations of metal ions.[7] Therefore, domain specialization may be a general property of monomeric LAGLIDADG homing endonucleases (as well as other DNA-binding proteins[8]), allowing rapid scanning and binding of B form DNA followed by specific stabilization of the kinked DNA conformations required for catalysis: an enzyme which bound only the bent conformations observed in the crystal structures would have binding kinetics limited by the population of rare DNA conformers, while one that bound only B form DNA would be incapable of catalysis.

---

[1] Scalley-Kim, M., McConnell-Smith, A., & Stoddard, B. L. Coevolution of a homing endonuclease and its host target sequence. *J. Mol. Biol.* **372**, 1305-1319 (2007)

[2] Silva, G. H., Dalgaard, J. Z., Belfort, M. & Van Roey, P. Crystal structure of the thermostable archaeal intron-endoded endonuclease I-DmoI. *J. Mol. Biol.* **286**, 1123-1136 (1999)

[3] Macaida, M. J. *et al.* Crystal structure of I-DmoI in complex with its target DNA provides new insights into meganuclease engineering. *Proc. Natl. Acad. Sci. U. S. A.* **105**, 16888-16893 (2008)

[4] Crothers, D. M. DNA curvature and deformation in protein-DNA complexes: a step in the right direction. *Proc. Natl. Acad. Sci. U. S. A.* **95**, 15163-15165 (1998)

[5] Silva, G. H., Belfort, M., Wende, W. & Pingoud A. From monomeric to homodimeric endonucleases and back: engineering novel specificity of LAGLIDADG enzymes. *J. Mol. Biol.* **361**, 744-754 (2006)

[6] Perrin, A., Buckle, M. & Dujon, B. Asymmetrical recognition and activity of the I-SceI endonuclease on its site and on intron-exon junctions. *EMBO Journal 12*, 2939-47 (1993)

[7] Turmel, M., Mercier, J. P., Cote, V., Otis, C. & Lemieux, C. The site-specific DNA endonuclease encoded by a group I intron in the Chlamydomonas pallidostigmatica chloroplast small subunit rRNA gene introduces a single-strand break at low concentrations of Mg2+. *Nucleic Acids Res* **23**, 2519-25 (1995)

[8] Kalodimo, C. G., Boelens, R. & Kaptein, R. A residue-specific view of the association and dissociation pathway in protein-DNA recognition. *Nat. Struct. Biol.* **9**, 193-197 (2002)